Dust Bands in the Asteroid Belt

M. Sykes
R. Greenberg
S. Dermott
P. Nicholson
J. Burns
T. N. Gautier

University of Arizona
Steward Observatory
Tucson, AZ 85721

8 September 1989

Scientific Report No. 1

APPROVED FOR PUBLIC RELEASE; DISTRIBUTION UNLIMITED

89 10 23 088

"This technical report has been reviewed and is approved for publication"

Paul D. LeVan
(Signature)
PAUL D. LEVAN
Contract Manager

Price
(Signature)
STEPHAN D. PRICE
Branch Chief

FOR THE COMMANDER

R. Earl Good
(Signature)
R. EARL GOOD
Director

This report has been reviewed by the ESD Public Affairs Office (PA) and is releasable to the National Technical Information Service (NTIS).

Qualified requestors may obtain additional copies from the Defense Technical Information Center. All others should apply to the National Technical Information Service.

If your address has changed, or if you wish to be removed from the mailing list, or if the addressee is no longer employed by your organization, please notify CL/IMA, Hanscom AFB, MA 01731. This will assist us in maintaining a current mailing list.

Do not return copies of this report unless contractual obligations or notices on a specific document requires that it be returned.

REPORT DOCUMENTATION PAGE

1a. REPORT SECURITY CLASSIFICATION UNCLASSIFIED	1b. RESTRICTIVE MARKINGS
2a. SECURITY CLASSIFICATION AUTHORITY	3. DISTRIBUTION/AVAILABILITY OF REPORT Approved for public release; Distribution Unlimited
2b. DECLASSIFICATION/DOWNGRADING SCHEDULE	

4. PERFORMING ORGANIZATION REPORT NUMBER(S)	5. MONITORING ORGANIZATION REPORT NUMBER(S) GL-TR-89-0262

6a. NAME OF PERFORMING ORGANIZATION Steward Observatory	6b. OFFICE SYMBOL (If applicable)	7a. NAME OF MONITORING ORGANIZATION Air Force Geophysics Laboratory
6c. ADDRESS (City, State, and ZIP Code) University of Arizona Tucson AZ 85721		7b ADDRESS (City, State, and ZIP Code) Hanscom AFB, MA 01731-5000

8a. NAME OF FUNDING/SPONSORING ORGANIZATION	8b. OFFICE SYMBOL (If applicable)	9. PROCUREMENT INSTRUMENT IDENTIFICATION NUMBER F19628-87-K-0045

8c. ADDRESS (City, State, and ZIP Code)	10. SOURCE OF FUNDING NUMBERS			

	PROGRAM ELEMENT NO.	PROJECT NO.	TASK NO.	WORK UNIT ACCESSION NO.
	63220C	S321	18	AB

11 TITLE (Include Security Classification)

(U) Dust Bands in the Asteroid Belt

12. PERSONAL AUTHOR(S)
Sykes, M., Greenberg, R., Dermott, S., Nicholson, P., Burns, J., and Gautier, T.N.

13a. TYPE OF REPORT Scientific #1	13b. TIME COVERED FROM _____ TO _____	14. DATE OF REPORT (Year, Month, Day) 1989 SEP 8	15. PAGE COUNT 40

16. SUPPLEMENTARY NOTATION

To appear in Asteroids II, Univ. of Ariz. Press

17. COSATI CODES			18. SUBJECT TERMS (Continue on reverse if necessary and identify by block number)
FIELD	GROUP	SUB-GROUP	Infrared
03	01		Solar System
03	02		Interplanetary Dust

19 ABSTRACT (Continue on reverse if necessary and identify by block number)

In 1983 the Infrared Astronomical Satellite (IRAS) discovered three bands of dust: one above, below, and approximately in the plane of the ecliptic. These bands are located in the asteroid belt and are believed to arise from collisional activity. Debris from an asteroid collision, over time, fills a torus having peaks in particle number density near its inner and outer corners, corresponding to the locus of perihelia and aphelia, respectively. As a consequence of this geometry, such a swarm should produce two pairs of bands that straddle the ecliptic - a perihelion band pair and an aphelion band pair (which generally overlap along the line of sight from earth). Indeed, processing of the IRAS data now resolves the band structure into at least three such band pairs, with indications of several more pairs distributed over a large range of ecliptic latitudes. Some of these bands appear to be associated with major Hirayama asteroid families, while others are not. Possible

20. DISTRIBUTION/AVAILABILITY OF ABSTRACT ☒ UNCLASSIFIED/UNLIMITED ☐ SAME AS RPT. ☐ DTIC USERS	21. ABSTRACT SECURITY CLASSIFICATION UNCLASSIFIED
22a. NAME OF RESPONSIBLE INDIVIDUAL Paul D. Levan	22b. TELEPHONE (Include Area Code) (617) 377-4550 22c. OFFICE SYMBOL AFGL/OPC

DD FORM 1473, 84 MAR
83 APR edition may be used until exhausted.
All other editions are obsolete.

origins of the observed dust bands include: (1) the gradual comminution of the asteroid belt as a whole, in which the local dust population is maximum where the concentration of asteroids is greatest (e.g. families); (2) one or a few large random asteroid collisions enhancing the local population of small debris, which in turn is comminuted into dust; and (3) the disintegration of one or more large comets. Dust bands are not necessarily constant features of the solar system. They form, gradually fade, and may be replenished, but estimates of time-scale and frequency are model dependent. Also, within the context of a given model, observations of dust bands may constrain the collisional history of the asteroid belt, including asteroid family ages, and may provide information on small-particle dynamics. Interpretation of the distribution of bands suggests that collisions in the asteroid belt are the principal source of zodiacal dust, transported to the vicinity of the earth by Poynting-Robertson drag.

I. INTRODUCTION

A. The Discovery of the Zodiacal Dust Bands

One of the major discoveries of the Infrared Astronomical Satellite (IRAS) was of three parallel bands of dust roughly straddling the plane of the ecliptic (Low *et al.*1984). Zodiacal dust bands were first noticed in the IRAS data as a pair of symmetrically placed bumps of 12 and 25 micron emission superimposed on the smooth zodiacal background (Figure 1). The same emission could be seen in the 60 and 100 micron data at a much lower intensity, indicating a fairly high temperature (about 200K) for the emitting material.

During its All-Sky Survey the IRAS telescope scanned the sky in circles of constant solar elongation, its nearly polar orbit precessing by $\sim 1°$ a day in order to remain above the terminator on the earth. The entire sky can be mapped over a period of six months in this way. More specifically, for the first two-thirds of its ten month life, IRAS used elongations between 80° and 100° to scan nearly the entire sky 4 times (Neugebauer *et al.*1984; IRAS Explanatory Supp. 1988). Each scan had a width of 0.°5, and was shifted in longitude by about 0.°25 on the subsequent orbit, observing by overlapping scans the same location twice after ~ 103 minutes. This was called an "hours-confirmed" observation or HCON. The initial observing strategy was to allow the telescope to map a section of sky in this fashion by slowly changing its solar elongation for about a week (HCON 1), after which the telescope was repositioned and the same section of sky was observed a second time (HCON 2).

As the sky survey unfolded, the emission bumps were found to be distributed more or less completely around the solar system. The initial impression was that two disks or belts of material had been found, presumably in the inner solar system because of their geometry and high color temperature. Such independent bands would, at some longitude, cross each other and the ecliptic. However, as the mapping became more complete the emission was found to form parallel bands above and below the ecliptic plane. They did not cross. This configuration was difficult to explain at first, since the upper and lower bands were thought *a priori* to be composed of separate groups of material which would have to cross the mid-plane given the Sun's central force. IRAS Science Team member D. Beintema suggested the correct explanation: A band pair can arise from a single distribution of material with an ensemble of orbits which shared a common inclination, but whose nodes were uniformly distributed over all ecliptic longitudes. This distribution produces a band pair because each individual particle spends most of its time at its extreme separation from the ecliptic, travelling roughly parallel to the plane, much like a pendulum is preferentially found at its maximum amplitude. A particle spends little time near the ecliptic plane because there it has a large velocity component normal to the plane.

A high-pass spatial filter can be employed to remove the smooth zodiacal background from the IRAS survey scans, revealing many details of the zodiacal dust bands. This process was used to produce the emission maps shown in Figure 2. The originally recognized band pair (γ) is seen $\sim 10°$ above and below the ecliptic. Part of the central

band is due to the peak in the smooth zodiacal emission near the plane leaking through the high-pass filter, but there is also clearly another pair of bands similar to the 10° bands, but spaced only one or two degrees from the ecliptic plane. These inner bands were later separated further into two pairs of bands (Sykes 1986).

Further analysis of the IRAS data has suggested that four additional pairs of bands may also exist (Table I) (Sykes 1988), and that these bands extend over 40° of ecliptic latitude. In the IRAS skyflux maps the central bands (α and β) have apparent widths of < 0°.5. The other bands, particularly the γ bands, are several degrees in apparent width (Sykes 1988). As will be seen later, the broad morphology of most dust bands has a significant impact on the number of bands which are possible to observe. So, from the original three bands reported by Low et al.(1984), as many as 14 bands (7 pairs) have now been detected.

B. Initial Analysis

During its last months of operation, IRAS surveyed the sky a last time (HCON 3), but changed its scanning pattern to begin at extreme solar elongations of 60° and 120° and smoothly approach 90° elongation from both sides and then reverse the procedure until the whole sky was covered (Figure 2b). This map includes only 72% of the sky because the survey was prematurely terminated by liquid helium exhaustion aboard the satellite. The γ bands, in particular, show clear variation in their separation corresponding to changes in viewing geometry, and can be readily understood if the density enhancements giving rise to the bands are confined to a small range in distance from the sun, maintain a constant linear separation around their circumference, and lie outside the orbit of the earth. This variation in parallactic separation yielded heliocentric distances and proper inclinations for the observed band material of 2.3 AU and 8°.7 (Gautier et al.1984), 2.5 AU and 8°.1 (Hauser et al.1985), and 2.44 AU and 8°.4 (Dermott et al.1989). None give error estimates, but the values seem to be reasonably consistent.

Color temperature calculations by Low et al.(1984) produced values between 165 K and 200 K. A rapidly rotating graybody of this temperature would be located between 3.2 AU and 2.2 AU, well within the main asteroid belt, and is consistent with the locations determined by parallax. Consequently, it was suggested that the dust bands arose from small particles generated by collisions among asteroids (Low et al.1984). This idea was reinforced by an apparent association between the latitudes of the bands and the proper inclinations of some major Hirayama asteroid families (Dermott et al.1984), which are believed to have been produced by the catastrophic disruptions of large asteroids (Table II). At the same time, Sykes et al.(1984) calculated that the random catastrophic disruption of a small asteroid (10 km in diameter) could possibly generate sufficient debris to be observed by IRAS as a band pair.

Models for the asteroidal origin of the dust bands has since followed two general paths which will be examined in more detail later. The first path (Dermott et al.1984,1985,1986,1988,1989) assumes the asteroid belt to be in collisional equilibrium, and that the size distribution of the particle population at all locations within the asteroid

belt is characterized by a power law with a single index over all sizes from tens of kilometers 'ɔ tens of microns. The surface area of dust at any given location thus increases monotonically with the local volume of asteroids. Since asteroid families represent concentrations of asteroids in $a - \sin i$ space, there should be corresponding peaks in the dust population. Hence, dust bands should be associated with asteroid families.

The second path (Sykes and Greenberg 1986; Sykes 1986,1988,1989) is a nonequilibrium theory of dust band origin which asserts that occasional random catastrophic disruptions of asteroids results in debris whose subsequent comminution products give rise to the dust bands. In this case dust bands are not associated with known asteroid families *a priori*, and may be found at other locations. This model predicts that dust bands should fade with time, and that the population of dust bands is replenished by new collisions. Though focussing on the more frequent disruptions of asteroids tens of kilometers in diameter, this model predicts that bands arising from disruptions large enough to create the largest Hirayama families should be detectable by IRAS for ≥ 1 Gyr.

An alternative theory for dust band origin is the disintegration of a large comet, which will be considered separately in this chapter (Sec. III.C). This comes about from the fact that the potentially most prominent cometary suppliers of the zodiacal cloud have similar inclinations to dust bands (Dermott *et al.*1984).

In the next section a mathematical model of a dust-band torus will be presented to provide some insight into what we are studying in terms of a spatial distribution of particles. The effects of secular gravitational perturbations and dispersions in orbital elements on this spatial distribution are then considered, which provide additional means of determining dust band locations as well as determining the effects of different physical processes on the small-particle population comprising a dust band. The different origin scenarios described above are presented, along with their observational consequences. Within the context of the (non-equilibrium) random collision hypothesis, we examine how dust bands form, how their surface areas decrease with time, and how many dust bands are likely to be seen as old bands are replaced by newer ones from more recent catastrophic disruptions.

II. THE DUST BAND TORUS

A. An Analytical Model

The spatial distribution of the dust we see as a dust band pair can be idealized by considering an ensemble of dust particles whose orbits have identical semi-major axes (a), proper eccentricities (e), and proper inclinations (i), but perihelia and nodes distributed over all longitudes. For purposes of exposition here, we neglect, for the moment, the effects of secular gravitational perturbations. The material fills a torus whose particle number density is (Sykes 1989)

$$\rho(r,\beta) = R(r)\Theta(\beta) \tag{1}$$

where

$$R(r) = \frac{C_r}{r^2 a} \left[\frac{r}{2a - r} \right]^{1/2} \left[1 + \frac{a^2(1 - e^2)^2}{e^2 r^2 - [a(1 - e^2) - r]^2} \right]^{1/2} \tag{2}$$

$$\Theta(\beta) = [2\pi^2]^{-1}[\cos^2\beta - \cos^2 i]^{-1/2} \tag{3}$$

within the limits

$$a(1 - e) \leq r \leq a(1 + e) \tag{4}$$

$$-i \leq \beta \leq i \tag{5}$$

Here C_r is a constant of normalization, r is heliocentric distance, and β is the heliocentric latitude with respect to the plane of symmetry (which is close to the ecliptic plane).

These equations describe a spatial distribution that is a torus with a squarish cross-section (Figure 3a), centered on the sun, whose radial extent is bounded by the perihelion and aphelion distances, and whose latitudinal extent is bounded by the proper inclination of particle orbits. Maxima in volume density occur at the "corners" of the torus. The latitudes of the maxima, seen from the sun, correspond to the proper inclination of the particle orbits. That is why, from the earth, these concentrations appear as pairs of bands straddling the ecliptic. The geometry is such that maxima in volume density at perihelion and aphelion give rise to both perihelion and aphelion band pairs (see Dermott et al.1985), which overlap each other when seen from the Earth. However, IRAS detects more flux from perihelion bands for two reasons: larger particle number densities and higher temperatures.

B. The Effects of Dispersions in Orbital Elements

Particles that make up a dust band torus do not have identical a, e, and i; there must be some dispersion in orbital elements. This significantly affects the spatial density of dust band particles (Figure 3b), and hence the locations at which their flux is seen. Two mechanisms by which the orbital elements of dust-band particles are distributed will be examined. The first mechanism is the collisional production of dust, considered in the next section. The second, considered in the section following, is Poynting-Robertson drag.

Collisional Dispersion. Studies of collision ejecta indicate that smaller particles tend to have larger ejection velocities (Melosh 1989), which yields a greater dispersion in orbital elements for small particles than large particles. Moreover, in a plausible particle size distribution (steeper than 1/diameter), small particles experience more collisions with other objects of comparable size than do large particles. The orbital elements of small particles will spread, consequently, more rapidly than large particles The most obvious effects are associated with a distribution in orbital inclinations, which primarily determines the angular separation of the bands we observe. For a Gaussian distribution with fixed mean values, increasing the dispersion in proper inclinations results in (a) increased band

widths and (b) shifting peak emission of the latitudinal profile to lower latitudes (Sykes 1989; Figure 4a). Thus, in the case of an asteroid family, a pair of bands consisting of associated dust having submillimeter diameters would be expected to be observed at lower latitudes than if the dust band particles had a distribition of orbital inclinations identical to kilometer and larger family members.

In general, the outer edge of an individual band (defined as the latitude where peak flux drops by half) increases slightly (Δ_+) with respect to the mean inclination of particle orbits with increasing dispersion in inclination, δi. Similarly, the latitude of the peak flux and inner band edge (defined as the latitude where the flux equals the average of the values at the midplane and peak) are displaced away from the mean inclination towards the midplane by Δ_0 and Δ_-, respectively. The empirical relations describing these shifts are (Sykes 1989):

$$\frac{\Delta_+}{i} \approx 0.48 \left(\frac{\delta i}{i} \right)^{0.89} \tag{6}$$

$$\frac{\Delta_0}{i} \approx 1.16 \left(\frac{\delta i}{i} \right)^{1.13} \tag{7}$$

$$\frac{\Delta_-}{i} \approx 1.73 \left(\frac{\delta i}{i} \right)^{0.84} \tag{8}$$

Another effect that can be seen in Figure 4 is the decreasing contrast of the inner edges of the bands with increasing dispersion in inclination. The ratio of peak flux (F_P) to the flux at the midplane (F_C) is approximated by

$$\frac{F_P}{F_C} \approx 0.71 \left(\frac{\delta i}{i} \right)^{0.5} \tag{9}$$

a factor of 2 lower than the upper limit of $1.414/\sqrt{\delta i/i}$ determined by Dermott et al.(1985). The relations (6) through (9) are good to within a few percent for $i < 20°$ and $\delta i/i \leq 0.25$.

Dispersions in semi-major axis and eccentricity act to increase the heliocentric distance of the peak flux from the perihelion bands while decreasing it for the aphelion bands (Figures 4b and c). Perihelion and aphelion bands associated with asteroid families overlap along the line of sight when observed from the earth, since the latitudinal displacement of their peaks is small. Increasing dispersion in semi-major axis and eccentricity thus decreases an already small peak-to-peak separation.

Dispersion Due to Poynting-Robertson Drag. The thermal flux from the dust bands is due principally to those particles in the 10 to 100 micron size range because of their greater surface area (Sykes and Greenberg 1986; Dermott et al.1986), and it is possible that the

orbits of these particles decay significantly due to Poynting-Robertson drag before they are either dynamically scattered (Dermott *et al.*1986) or are comminuted to sizes which are ejected from the immediate vicinity by radiation pressure (Sykes 1989). If orbital decay is significant, then the particles in the dust bands will have a wide range of semi-major axes, and may show significant dispersions in proper eccentricity and inclination, forced inclination, and forced ascending node (these "forced" elements are functions of semi-major axis and will be discussed more fully in Sec. II.C below). These dispersions arise from two causes: (1) Passage through various resonances, particularly the 1:3 gap at 2.5 AU, results in a dispersion of the proper eccentricities and inclinations (Dermott *et al.*1989). (2) If the particles have a range of semi-major axes, then they must also have a range of forced orbital elements (cf. Figure 5). This may be particularly important for those particles close to the inner edge of the asteroid belt ($a < 2.5$ AU), and it may be that the dispersion of the orbital elements in this region of the belt defines the inner edges of the dust bands if the particle orbits have decayed (Dermott and Nicholson 1989).

The effect of dispersion due to Poynting-Robertson drag is not the same as collisional dispersion (where the mean orbital elements are unchanged). In the former case, the shift in the peak dust band emission to higher or lower ecliptic latitudes is a function of the longitude of observation (Sykes 1989). Also, a simple decrease in the heliocentric distance of dust pericenters results in an increase in the apparent angular separation of a band pair as a consequence of parallax.

C. The Effects of Secular Gravitational Perturbations

A careful examination of the dust-band images in ecliptic coordinates (Figure 2) shows that they are not symmetric about the plane of the ecliptic. The orbits of the dust-band particles are perturbed by Jupiter and other planets whose orbits are slightly inclined to the ecliptic. Ensembles of particles with the same semi-major axes will precess about a common plane where the torques produced by these gravitational perturbations vanish. This defines the plane of symmetry of the dust-band torus which has an inclination relative to the ecliptic) i_f and ascending node Ω_f which vary with semi-major axis (Figures 5a and b). These gravitational perturbations also act to distort particle orbits, introducing a "forced" component to their eccentricities. Some of the effects of this on the dust-band torus are shown in Dermott *et al.*(1985). The torus shifts away from its sun-centered position by an amount ae_f in a direction opposite to that of $\tilde{\omega}_f$ (Figure 5c), which now defines the longitude of pericenter of the torus. Figures 5b and d show the variations in these parameters as a function of semi-major axis. We see that as the semi-major axis moves closer to Jupiter (the dominant perturber) beyond 2.6 AU, these forced element components approach values for Jupiter's orbit. The shifting of the torus center gives rise to a longitudinal temperature variation in the bands which are diagnostic of their distances (Dermott *et al.*1985).

The existence of these various effects allows for the potential extraction of all the orbital elements of the dust band particles. Semi-major axis can be determined by the direct measurements of Ω_f and $\tilde{\omega}_f$. The use of Ω_f in this way is described for the β bands

in Section III.A. The apsidal longitude $\tilde{\omega}_f$ is that at which dust-band temperatures are highest. Given the semi-major axis of the torus particle orbits, their proper eccentricity and forced eccentricity can be decoupled through the longitudinal variation of dust band temperature (Dermott and Nicholson 1989). The proper inclination and forced inclination of the dust bands can be decoupled from measurements of band center latitudes and band separation as a function of longitude (Dermott *et al.*1989; Sykes 1989). Secular gravitational perturbations also result in the distortion of the dust band torus, resulting in the north and south bands no longer being exactly plane parallel. Determining the angle between the planes containing the individual bands making up a band pair provides another means of calculating the forced eccentricity (Sykes 1989).

III. THE ORIGIN OF THE DUST BANDS

A. The Collisional Equilibrium (Asteroid Family) Hypothesis

This hypothesis assumes that the dust population at a given location is related to the population of observatble asteroids at the same location. This has been examined by assuming that, at each point in the asteroid belt, all sizes of particles are characterized by a single equilibrium size distribution arising from the general comminution of the asteroid belt through mutual collisions. This model predicts that prominent dust bands are associated with known concentrations of asteroids such as the asteroid families. By demonstrating a relationship between dust bands and asteroid families, the equilibrium hypothesis provides one vehicle by which dust production can be understood in the asteroid belt as a whole, as well as its relationship to the observed zodiacal dust complex.

The relationship between the Hirayama asteroid families and the prominent dust bands has been a central question in the study of the latter since it was first posed by Dermott *et al.*(1984). In the following, the consistency between the calculated surface areas and volumes of the dust bands and the major Hirayama asteroid families is examined. Two basic approaches are then taken to determine whether the dust bands derive from asteroid families. The first method is the direct (or indirect) measurement of some of the orbital elements of the dust bands. These can then be compared with the corresponding elements of the asteroid families. The second method is the generation of predictive models which are then compared with the IRAS dust band observations.

Estimating Dust Band Volume. The surface optical depth of the prominent dust bands was estimated to be $\sim 10^{-8}$ (Low *et al.*1984), corresponding to a total surface area of $\sim 2 \times 10^{19}$ cm^2 (Dermott *et al.*1984). It is assumed that the size-frequency distribution of the dust band particles is described by a single power law of the form

$$dN(m) = Km^{-q}dm \qquad (10)$$

where dN is the number of particles having masses between m and $m+dm$, K is a constant,

and q is the mass index. Following Dermott and Nicholson (1989), this converts to the following cumulative power law in radius,

$$N(r) = \frac{1}{3(q-1)} \left(\frac{r_0}{r}\right)^{3(q-1)} \tag{11}$$

where $N(r)$ is the number of asteroids with radii $> r$ and r_0 is a constant, similar in magnitude to the largest particle (in this case asteroid) radius. The total area, A, of the particles is then given (for $q > 5/3$) by

$$A = \frac{\pi r_{min}^2}{(3q-5)} \left[\frac{r_0}{r_{min}}\right]^{3(q-1)} \tag{12}$$

where r_{min} is the lower cut-off in the size distribution, while the total volume of the particles, V, can be obtained from the radius, R_e, of a sphere with the same volume. $V = (4/3)\pi R_e^3$ and, to a good approximation (for $q < 2$),

$$R_e = r_0[3(2-q)]^{-1/3}. \tag{13}$$

Values of R_e that are needed to account for the observed areas are shown in Figure 6 for a range of values of r_{min} and q. The theoretical equilibrium solution for asteroids (Dohnanyi, 1978) has a population index $q = 1.837$ (indicated by the vertical line in Figure 6). If q is in the vicinity of this value, and the size-distribution extends down to $\sim 10\mu m$, then we can conclude from Figure 6 that spheres containing the inferred volume of dust band particles (up to asteroids tens of kilometers in radius) must have equivalent radii of ~ 100 km. The equivalent radii shown in Figure 6 are similar to the radii of Hirayama family progenitors (Gradie et al.1979; Dermott et al.1984). Assuming a single size-frequency index, however, does result in large variations in surface area produced by a given mass of material if the index or minimum particle size is varied. In a non-equilibrium case (Section III.B.; Sykes and Greenberg 1986) the initial population index may be close to $q = 2$. Subsequent evolution calculated by Sykes and Greenberg (1986) shows that the population quickly changes from the initial power-law. The result is that much smaller bodies (with equivalent radii of ~ 10 km) could be dust band parents, and numerical experiments indicate that the theory is not very sensitive to the initial value of q.

Measuring Dust Band Orbital Elements. The simplest means of determining the semi-major axes of dust band particles is to determine the orientation and/or the inclination of their plane of symmetry relative to the ecliptic. Utilizing different methods, contradictory results have been obtained for the central dust bands.

Using the $0°.5$ IRAS Zodiacal History File (ZOHF) (see IRAS Explanatory Supp. 1988), Dermott et al.(1988) separated dust-band profiles from the broad zodiacal background utilizing a Fast Fourier Transform and high-pass filtering with a Parzen window. Plotting the latitude of the central dust band (Figure 7), in which the α and β bands are

not resolved, it was estimated that the forced inclination of the composite central band is 1°.2 and that the longitude of the associated ascending node is 52°. The forced inclination clearly differs from that of the zodiacal cloud (1°.5) and is what one would expect for the Themis (at $a = 3.1$ AU) and Koronis (at $a = 2.9$ AU) asteroid families (see Figure 5). However, the node is the same as that of the background cloud and disagrees with the expected longitude of $\sim 97°$ for particles at a distance of 3 AU (Figure 5).

A parallactic measurement (Figure 8) of the resolved β band pair was obtained by Sykes (1989) using the IRAS Skyflux Maps (IRAS Explanatory Supp. 1988). The proper inclination of the particle orbits measured was 2°.1 , consistent with the Koronis asteroid family. Sykes found the ascending node for this band pair to be $90° \pm 6°$, reasonably consistent with the value of 96° expected for particles with the semi-major axes of the Koronis family. The discrepancy with the earlier measurement is thought by Sykes (1989) to arise from the contamination of Fourier-filtered dust-band profiles of Dermott *et al.*(1988) by a possible cusp-like high-spatial frequency component of the broad zodiacal emission.

Comparison with Family Dust-Band Models.   Dermott and Nicholson (1989) have constructed a three-dimensional numerical model that permits the calculation of the distribution of night-sky brightness that would be produced by any particular distribution of dust-particle orbits. This model includes the effects of planetary perturbations on the dust-particle orbits, reproduces the exact viewing geometry of the IRAS telescope, and allows for the eccentricity of the earth's orbit. The result is a model for the variation with ecliptic latitude of the brightness observed in a given waveband as the line of sight of the telescope sweeps through the model dust bands at a constant elongation angle. The models assume the same dispersion in orbital elements as that displayed by the known family members. In Figure 9 this model is used to generate a predicted profile for the Eos and Themis asteroid families and is compared with a high-pass filtered scan from the Zodiacal History File. The model distributions for the asteroid families are too sharply peaked to account for the observed profiles. Dermott and Nicholson then examine the effects of dispersion due to evolution under Poynting-Robertson drag, and this yields some improvement in the comparison of model and filtered profiles. However, while the agreement between observed dust bands and specific models of orbitally evolved particles originating in the prominent Hirayama families is sugges* , defini,ive results from this approach are not yet available.

Sykes (1989) uti; · the dust band model of Sec. II and maps the inner and outer edges of the la,itu, profile of the dust bands as well as the location of peak emission onto the two-dimens;,- il IRAS Skyflux Maps. This allows the α and β bands to be individually studi^d (F , ;e 10a), whereas they are indistinguishable at the lower resolution of the Zodiaca, "istory File. Like Dermott and Nicholson (1989), Sykes initially assumes that the mean orbital elements of the dust band particles are the same as the corresponding family members. The only parameter varied is the dispersion in proper inclination which is assumed to be gaussian. Separations between perihelion and aphelion bands are found to be small, and increasing dispersions in semi-major axis and eccentricity only makes that separation smaller. Mapping routines fully reproduce the IRAS pointing

geometry.

Comparison of Koronis and Themis models with the β and α bands, respectively, yields excellent fits to the data as observed in the IRAS Skyflux Maps at all longitudes (Figure 10b,c). This assumes increased dispersions in proper inclinations of less than a factor of two for the model Koronis bands and a little greater than two for the model Themis bands. Modifying the Koronis and Themis family models by decreasing the semi-major axis and other associated orbital elements (including "forced" components) consistent with orbital decay by Poynting-Robertson drag, results in significant divergence from the observed locations of the α and β bands. At $a = 2.4$ AU, the discrepancy can be as large as $1°5$ in latitude. This compares with a width of $\sim 1/4°$ for the β bands in the IRAS Skyflux plates.

The γ bands are very closely tracked by the model Eos bands in the filtered Zodiacal History File images (cf. Figure 1), indicating an orientation and inclination of the γ torus that may be similar to that of the Eos family. However, the Eos family band model yields a latitude of peak emission which is systematically greater than that observed for the γ bands. Also, the pericenter distances of the bands determined by parallax (Section I.B) indicate a value ~ 0.4 AU smaller than that of Eos family members. The former may be resolved by increasing the dispersion in proper inclinations of the model Eos bands by a factor of ~ 2. This also results in significant broadenning of the bands (Figure 3), which seems to agree with the several degree width of the individual γ bands (Sykes 1989). Dispersion due to Poynting-Robertson drag (section II.B) may also account for band broadenning and and a decrease in apparent latitude (Dermott et al.1989), though such effects are viewing-geometry dependent and may not occur at all longitudes observed (Sykes 1989). On the other hand, the apparent discrepancy in pericenter distances may be explained by the Poynting-Robertson drag. An alternative explanation in both cases is that the γ bands and Eos asteroid family are not causally related.

In addition to the more prominent α, β, and γ bands, fainter dust bands reported by Sykes (1988) (Table I) were compared to model bands associated with several other known asteroid families (Table II). This resulted in a possible correlation between the Io family and the J/K bands (Sykes 1989). However, no bands were detected in association with the Flora, Nysa, or Maria families. Flora and possible Maria bands had been predicted previously on the basis of the collisional equilibrium hypothesis (Dermott et al.1985). Their absence coupled with the apparent existence of bands not associated with any prominent asteroid families present a challenge to the collisional equilibrium hypothesis of dust band origin.

B. The Non-Equilibrium (Random Collision) Hypothesis

The asteroid belt contains tens of thousands of objects in mutual-crossing orbits. On average, the population of particles may be described by some equilibrium size-frquency distribution as discussed in the previous section. However, when two asteroids collide, a small area of orbital element space will be filled with their debris. As this debris experiences further collisions with background interplanetary dust particles (IDP's), the local dust

population will be enhanced. If the collision is large enough, the resultant dust population deriving from the comminution of its debris, may have enough surface area to be detected by an instrument such as IRAS. Eventually, removal of dust through radiation forces and the continual erosion of the debris population results in the decline of the surface area of dust. Then at another location, another collision takes place and the process is repeated.

The nonequilibrium, or random collision, hypothesis of dust band origin views dust bands as the product of a stochastic process in which they are created and destroyed over geologic time, while maintaining a certain average population whose spatial distribution may be different at different times. This is in contrast to the equilibrium hypothesis, in which the dust band population and spatial distribution is effectively steady-state.

In the following subsections, some of the consequences of the non-equilibrium model are examined: band pairs must form on finite timescales; their surface area changes with time as mass is collisionally redistributed from larger sizes to smaller, a pseudo-equilibrium population of bands must be maintained due to constant "gain" and "loss" rates. Finally, predictions grounded in the non-equilibrium hypothesis must be tested against the IRAS data.

Dust Band Formation. The collisional disruption of an asteroid results in fragments having a dispersion in semimajor axes that is likely small compared with the semimajor axis of the parent body. For example, the major Hirayama families (Gradie *et al.*1979) have a dispersion of semi-major axes corresponding to relative orbital velocities of ~ 100 m/s, compared with absolute orbital velocities of ~ 17 km/s. In fact, it is a mystery how even a value as great as 100 m/s could have been achieved. Such a small dispersion in semimajor axes results in these debris being distributed around the orbit of the parent body on time scales of $\sim 10^3$ years.

The orbits of asteroids (and therefore debris in the asteroid belt) experience secular precession of their apsides and nodes as a consequence of gravitational perturbations by Jupiter and the other planets. The dust-band torus is formed as the orbits of collisional debris precess at different rates due to small differences in their orbital elements, primarily semi-major axis, so that with time their nodes spread around the ecliptic relative to each other. Two mechanisms operate simultaneously to distribute the nodes of particle orbits. The first is differential precession due to the differences in semi-major axes for particles of a given size. The second is a mass fractionation of the nodes arising from the size-dependent variation of semi-major axes with time due to Poynting-Robertson drag on smaller particles (Sykes and Greenberg 1986).

Increasing the dispersion in semimajor axes increases the rate at which band pairs are formed by this mechanism, as does increasing the mean semimajor axis of the particle orbits. This last is a consequence of the stronger gravitational effects of Jupiter as the particle orbits approach Jupiter's orbit. From Figure 11, minimum formation timescales range between 10^5 and $\sim 10^7$ years, with dust bands associated with the Themis, Koronis, and Eos families forming in less than 10^6 years.

Mass fractionation of the orbital nodes occurs as Poynting-Robertson drag decreases the semi-major axis of small particles with time, relative to large particles. Small

particles consequently precess at increasingly lower rates with respect to large particles. Depending on the size-frequency distribution of particles created in the initial catastrophic disruption, this mechanism can potentially result in more rapid band pair formation ($\sim 10^5$ to 10^6 years) than differential precession due to the initial dispersion in semi-major axes (Figure 12).

Surface Area Evolution. The debris that comprises a dust-band torus will not maintain its original mass distribution. Particles are comminuted by collisions with background interplanetary dust particles, both cometary and asteroidal in origin. Catastrophic fragmentation, rather than gradual erosion, dominates the comminution (Dohnanyi 1978), and the breakup of larger particles into smaller particles increases the surface area of the dust bands, tending to increase their brightness. Mass (and surface area) from the torus is eventually lost when the debris is comminuted into small enough fragments that they are rapidly swept away by Poynting-Robertson drag or radiation pressure (Figure 13). For most meteoritic compositions this corresponds to particle diameters between approximately 0.08 and 4 microns (Burns *et al.*1979).

In the competition between production and loss rates of surface area in a dust band torus, gradual loss eventually wins out with time (Figure 13c). Thus, the eventual fate of any band pair in the non-equilibrium model is to fade away (Sykes and Greenberg 1986).

How Many Dust Bands Should We See? According to the nonequilibrium model, the population of bands above a limiting surface area will be determined by two quantities: the mean time between collisions occur which generate more than the minimum required surface area (the gain term), and the lifetime of bands before they fade below this limit (the loss term). The ratio of the gain to loss terms determines the number of bands one would expect to observe at any given time. Based on their models, Sykes and Greenberg (1986) calculated that there should be on the order of 2 pairs of bands with surface areas equal to or exceeding that estimated for the bands reported by Low *et al.*(1984) and $\sim$30 pairs of bands an order of magnitude fainter. This agreed nicely with the number of bands at the bright end (Low *et al.*1984), but seemed to conflict with the smaller number of faint bands detected by Sykes (1988). The problem was resolved when it was found that the dust bands are not sharp features, but have typical widths of a few degrees (the exception being the α and β bands. Assuming Gaussian profiles, Sykes (1988) showed that the superposition of so many faint and bright bands would produce something of a continuum above which only 2 to 5 bands (or clusters of bands) could be detected in addition to the α, β, and γ bands. Thus, the noneqilibrium model is consistent with the numbers of bands now detected.

The dust bands predicted by Sykes and Greenberg (1986) were disruption products of asteroids tending to have diameters between 5 and 10 km. A significant fraction of these bands also arose from the disruption of 30 to 90 km diameter bodies. Thus, the prominent α, β, and γ bands (with the possible exception of the β bands), assuming association with the Themis, Koronis, and Eos families, respectively, were not predicted by

Sykes and Greenberg (1986). Bodies large enough to form the Themis and Eos asteroid families disrupt so infrequently (on time scales of the age of the solar system) that they were not included in the collision statistics. However, the Sykes and Greenberg model can explain the observation of these bands in the event of such large collisional disruptions. This is due to their long observational lifetimes. At the other end of the scale, asteroids much smaller than 5 km in diameter would not produce enough debris to form a detectable band pair.

The mean time between catastrophic collisions generating a mass of debris equivalent to a 5-10 km asteroid was found to be 10^5 and 10^6 years – on the order of both the dust band formation time and lifetime (for surface areas exceeding 10^{18} cm^2, $\sim 1/10$ that of the prominent bands). Consequently, it was thought that faint partial band pairs might be observed (whose nodes were not distributed over all latitudes). Such a partial band was reported to be detected (Sykes 1986, 1987), but later evidence suggested that the structure had moved over a period of eight months, indicating that it may actually be a debris trail of a type not previously observed (Sykes 1988).

C. The Comet Hypothesis

It cannot be concluded *a priori* that because the zodiacal dust bands are located in the asteroid belt, that they have an asteroidal origin. Numerous short-period comets have low inclinations; the peak in the distribution of the observed inclinations is actually close to 10°. Many of the observed short-period comets also have perihelion distances between 2 and 4 AU and, because of selection effects, there is probably a large number of such comets with perihelia within the asteroid belt that remain undetected (Burns *et al.*1984; Dermott *et al.*1989).

IRAS discovered that m y short-period comets have associated dust trails detected over large portions of their orbits (Sykes *et al.*1986a). In Figure 1, the dust trails associated with P/Tempel 2 and P/Encke are clearly seen. This represents a possibly significant increase in the contribution of cometary dust to the zodiacal dust complex, particularly in the submillimeter and millimeter size ranges (Sykes *et al.*1986b). Another source of zodiacal dust of possible cometary origin are the Type II dust trails (*A* to *D* in Figure 1) (Sykes 1988). These recently detected structures may arise from the ejection of large particles at high velocities ($\sim$ 100 m/s) from a comet nucleus during perihelion passage, in comparison to the lower velocities ($<$ 10 m/s) associated with the originally detected Type I trails. They may also represent the breakup of cometary nuclei. In either case, the dust trail particles will tend to evolve into a dust band torus as described in Sec. III.B., though with a much greater radial width than for asteroid debris due to the larger typical cometary eccentricities.

As a torus forms, the cometary material is spread out over a substantially larger volume, tending to decrease the surface brightness of the dust observed unless it is increased through comminution of the larger particles or the emission of additional material from the parent comet. In the case of the latter, emissions from short-period comets are expected to last only about 10,000 orbits (the nominal lifetime of a short-period comet), which is

smaller than the dust band formation timescales. Unless the comet itself is disrupted, the population of large particles whose comminution provides the observed dust population is likely to be minimal. Therefore dust bands associated with cometary emission are likely to be very short-lived. There remains the possibility, however, that emissions from a large number of small, undetected short-period comets could superpose to yield an observable dust band torus.

The disruption of a cometary nucleus might allow for a dust band to be formed as bright as any detected by IRAS. Though highly uncertain, the size-frequency distribution of the large-particle population of comets is thought to have a size index $q \sim 2.1$ (Sekanina 1979). This is similar to the initial size distribution assumed for a catastrophically disrupted asteroid by Sykes and Greenberg (1986). From Figure 6, such breakup would require an initial cometary radius of only ~ 10 km, similar to that observed for Halley (Sagdeev et al.1986; Keller et al.1986). The frequency with which such cometary disruptions occur would then determine the probability of the resultant band pair being observed.

One means of distinguishing between asteroidal and cometary models of the bands is probably a combination of the forced orbital element and parallax methods (Dermott et al.1989). The forced orbital element method determines the semi-major axis of the particles, whereas the parallax method determines an "effective distance" which is probably closely related to the pericenter distance, $a(1-e)$. Thus, it should be possible, in principal, to determine the proper eccentricities of the particle orbits, thereby indicating whether the particles derive from comets.

IV. DISCUSSION

Neither the equilibrium nor non-equilibrium models of dust band origin, as currently formulated, present a complete picture of the IRAS dust band observations. The equilibrium model fails to explain the existence of bands at non-family locations and the absence of bands associated with the Flora, Nysa, and Maria families. Both theories explain the α, β, and γ bands and their respective relationships to the Themis, Koronis, and Eos families. The non-equilibrium model of Sykes and Greenberg (1986) overestimates the surface brightness of bands arising from the disruption products of small asteroids (unless it eventually turns out that γ bands are not associated with the Eos family). It also predicts the detection of partial bands, which have yet to be unambiguously observed.

On the other hand, the equilibrium model led to the initial correlation between the prominent bands and the major Hirayama asteroid families (Dermott et al.1984), and the non-equilibrium model inspired the search for and detection of zodiacal structures including additional dust bands (Sykes 1988). Both models predicted that a significant fraction of the zodiacal dust complex derives from the asteroid belt.

If the asteroid belt is a principal source of zodiacal dust, then that dust must be transported to the inner solar system by Poynting-Robertson drag. Initially, it seems contradictory that the previous statement be true while the dust bands - regions where

dust is obviously being generated - evidence little if any orbital decay (Hauser *et al.*1985; Dermott and Nicholson 1989; Sykes 1989). Sykes (1989) interprets these observations as indicating particle sizes whose collisional lifetimes are short in comparison with their Poynting-Robertson decay times, and that the removal of their comminution products from the ensemble of dust band particles must be rapid. This does not mean that the particles simply disappear, rather that they are no longer distinguishable from the broad zodiacal background depicted in Figure 1. One possibility is that a significant fraction of the smaller particles are comminuted into sizes sensitive to radiation pressure, which are then essentially removed from the ensemble of dust-band particles on timescales of an orbital period. These particles eventually decay by P-R drag, but their surface area is spread over a large volume and hence contribute little to the local dust-band surface brightness.

Dermott and Nicholson (1989) believe that P-R drag will turn out to explain the broadness of the bands and the apparent displacement of parallactic distances of the dust bands inward from the pericenters of their associated families.

The association of dust bands with asteroid families may help to shed some light on the nature and evolution of the latter. The major Hirayama families are thought to have originated with the breakup of large parent asteroids (Kuiper 1950). That the dust bands have orbital elements consistent with the mean elements of the corresponding families indicates (from the perspective of the non-equilibrium model) that we probably are looking at comminution products of debris from the original family-forming collision, rather than from the random disruption of a smaller family member (which would likely have a different inclination). Thus, the dust-band surface area evolution model can be utilized in an attempt to constrain the ages of asteroid families. This was done by Sykes (1986) utilizing the dust band surface area evolution model of Sykes and Greenberg (1986). A total surface area of 2×10^{19} was assumed for bands associated with the Themis, Koronis, and Eos families, which is probably something of an overestimate, particularly for the Themis family which have a relatively low surface brightness in the IRAS skyflux maps. A surface area of 10^{18} cm^2 was assumed as an upper limit to the dust in the Nysa family. The calculated times elapsed since the disruption of the family parent bodies are listed in Table III, and should be considered as very model dependent. If the calculated values are correct, this model indicates that the Koronis family is much younger than both the Themis and Eos family. This result is consistent with rotational studies of family members (Binzel 1987). If the Nysa family was the product of a catastrophic disruption, then its lack of an associated dust band suggests that a family-forming collision was indeed ancient.

The Sykes and Greenberg model says that dust bands deriving from the disruption of an asteroid on the order of a few hundred kilometers in diameter should be detectable by a detector like IRAS for at least 1 Gyr. Also, according to this model the probability of any such event occuring in the last several Gyr is very small. The fact that two such events are observed (Themis and Eos) and that other families with similar sized parents arose from even earlier collisions suggests two things: (1) collisional activity was much greater in the asteroid belt more than a billion years ago, or (2) many families may not have derived from a single collisional event, but that they may be associations aris-

ing from segregation or lumping (in orbital element space) as a consequence of dynamical resonances, such as the Phocaea family (Williams 1971).

IRAS first detected the dust bands in 1983, providing a new database and phenomenology against which models of asteroid collisional activity and small particle dynamics could be tested. A wealth of more information is yet to come as more spacebased infrared telescopes are launched (beginning with the Cosmic Background Explorer (COBE) in the fall of 1989, to be followed by the Infrared Space Observatory (ISO) in the 1990s and the Space Infrared Telescope Facility (SIRTF) early in the next century). The instruments being launched will allow not only for more detailed studies along lines reviewed here, but also will allow spectroscopy studies to be undertaken, opening whole new areas of investigation to link dust to asteroids and comets and link dust in the asteroid belt to extraterrestrial dust collected in the Earth's atmosphere and elsewhere.

REFERENCES

Binzel, R.P. (1987). Collisional evolution in the Eos and Koronis asteroid families: Observational and numerical results. *Icarus* **73**, 303-313.

Burns, J.A., Lamy, P., and Soter, S. (1979). Radiation forces on small particles in the solar system. *Icarus* **40**, 1-48.

Burns, J.A., Dermott, S.F., Nicholson, P.G., and Houck, J.R. 1984. IRAS' solar system dust rings: Collisional debris from asteroids or comet dust. IAU Colloquium 85, *Properties and Interactions of Interplanetary Dust*, Marseille, p. 72.

Dermott, S.F., Nicholson, P.D., Burns, J.A., and Houck, J.R. (1984). Origin of the solar system dust bands discovered by IRAS. *Nature*, **312**, 505-509.

Dermott, S.F., Nicholson, P.D., Burns, J.A., and Houck, J.R. (1985). An analysis of IRAS' solar system dust bands. In *Properties and Interactions of Interplanetary Dust*, ed. R. Geise and P. Lamy (Reidel), 395-409.

Dermott, S.F., Nicholson, P.D., and Wolven, B.A. (1986). Preliminary analysis of the IRAS solar system dust data. In *Asteroids, Comets, Meteors II*, ed. Lagerkvist, B.A., Lindblad, H., Lundstedt, H. and Rickman, H. (Uppsala), 583-594.

Dermott, S.F., Nicholson, P.D., Kim, Y., Wolven, B.A., and Tedesco, E.F. (1988). The impact of IRAS on asteroid science. In *Comets to Cosmology*, ed. A. Lawrence (Springer-Verlag), pp. 3-18.

Dermott, S.F. and Nicholson, P.D. (1989). IRAS dust bands and the origin of the zodiacal cloud. In *Highlights of Astronomy*, in press.

Dermott, S.F., P.D. Nicholson, R.S. Gomes, and R. Malhotra (1989). Modelling the IRAS solar system dust bands. *Adv. Space Res.*, in press.

Dohnanyi, J.S. (1978). Particle dynamics. In *Cosmic Dust*, J.A.M. McDonnell, ed. (Wiley, Chichester), pp. 527-625.

Gautier, T.N., Hauser, M.G., and Low, F.J. (1984). Parallel measurements of the zodiacal dust bands with the IRAS Survey. *B.A.A.S.*, **16**, 442.

Gradie, J.C., Chapman, C.R., and Williams, J.G. (1979). Families of minor planets. In *Asteroids* (T. Gehrels, Ed.). University of Arizona Press, Tucson. pp. 359-390.

Hauser, M.G., F.C. Gillett, F.J. Low, T.N. Gautier, C.A. Beichman, G. Neugebauer, H.H.

Aumann, B. Baud, N. Boggess, J.P. Emerson, J.R. Houck, B.T. Soifer, and R.G. Walker (1984). IRAS observations of the diffuse infrared background. *Ap. J. (Letters)*, **278**, L15-L18.

Hauser, M.G., Gautier, T.N., Good, J., and Low, F.J. (1985). IRAS observations of the interplanetary dust emission. In *Properties and Interactions of Interplanetary Dust*, ed. R. Giese and P. Lamy (Dordrecht: Reidel). pp. 43-48.

IRAS Explanatory Supplement (1988). eds. G. Neugebauer, H. Habing, P. Clegg, and T. Chester. (Washington D.C.: Government Printing Office).

Keller, H., C. Arpigny, C. Barbieri, R. Bonnet, S. Cazes, M. Caradini, C. Cosmovici, W. Delamare, W. Huebner, D. Hughes, C. Jamar, D. Malaise, H. Reitsema, H. Schmidt, W. Schmidt, P. Siege, F. Whipple, and K. Wilhelm (1986). First Halley Multicolor Camera imaging results from Giotto. *Nature* **321**, 320-326.

Kuiper, G. (1950), On the origin of asteroids. *Astron. J.* **55**, 164.

Low, F.J., D.A. Beitema, T.N. Gautier, F.C. Gillett, C.A. Beichman, G. Neugebauer, E. Young, H.H. Aumann, N. Boggess, J.P. Emerson, H.J. Habing, M.G. Hauser, J.R. Houck, M. Rowan-Robinson, B.T. Soifer, R.G. Walker, and P.R. Wesselius (1984). Infrared cirrus: new components of the extended infrared emission. *Astroph. J. (Letters)* **278**, L19-L22.

Melosh, H.J. (1989) *Impact Cratering.* Oxford University Press, New York.

Neugebauer, G., C.A. Beichman, B.T. Soifer, H.H. Aumann, T.J. Chester, T.N. Gautier, F.C. Gillett, M.G. Hauser, J.R. Houck, C.J. Lonsdaley, F.J. Low, and E.T. Young 1984, *Science* **224**, 14-21.

Sagdeev, R.Z., J. Blamont, A. Galeev, V.I. Moroz, V. Shapiro, V. Shevchenko, and K. Szego (1986). Vega spacecraft encounters with comet Halley. *Nature* **321**, 258-262.

Sekanina, Z. (1979). Expected characteristics of large dust particles in periodic comet Halley. In *Comet Halley Micrometeorite Hazard Workshop*, ed. N. Longdon (ESA SP-153), pp. 25-34.

Sykes, M.V., Greenberg, R., and Hunten, D. (1984). Formation of the zodiacal dust bands in the asteroid belt. *B.A.A.S.*, **16**, 690.

Sykes, M.V. and Greenberg, R. (1986). The formation and origin of the IRAS zodiacal dust bands as a consequence of single collisions between asteroids. *Icarus*, **65**, 51-69.

Sykes, M.V. (1986). *IRAS Observations of Asteroid Dust Bands and Cometary Dust Trails.* Ph.D. Thesis, University of Arizona.

Sykes, M.V., L.A. Lebofsky, D.M. Hunten, and F.J. Low (1986a). The discovery of dust trails in the orbits of periodic comets. *Science* **232**, 1115-1117.

Sykes, M.V., D.M. Hunten, and F.J. Low (1986b). Preliminary analysis of cometary dust trails. *Adv. Space. Res.* **6**, 67-78.

Sykes, M.V. (1987). Evidence for a recent catastrophic asteroid collision. *Bull. Am. Astr. Soc.* **19**, 825.

Sykes, M.V. (1988). IRAS observations of extended zodiacal structures. *Ap. J. (Letters)* **334**, L55-L58.

Sykes, M.V. (1989). Zodiacal dust bands: their relation to asteroid families. *Icarus*, submitted.

Williams, J.G. (1971). Proper elements, families, and belt boundaries. In *Physical Studies of Minor Planets*, ed. T. Gehrels (NASA SP-267, Washington D.C.: U.S. Government Printing Office), pp. 177-181.

Williams, J.G. (1979). Proper elements and family memberships of the asteroids. In *Asteroids*, ed. T. Gehrels (Tucson: University of Arizona Press), pp. 1040-1063.

Table I. Dust Band Pairs

Name	Geocentric Ecliptic Latitude (HCON 1 and 2)	Comments
α	±(0 to 2.5)	Unresolved with β (Low *et al.*1984). Resolved ans associated with Themis family (Sykes 1986).
β	±(1 to 3.5)	Unresolved with α (Low *et al.*1984). Resolved and associated with Koronis family (Sykes 1986).
γ	±(8.5 to 11.5)	Low *et al.*, 1984. Associated with Eos family (Dermott *et al.*1984).
E	4 to 6	Possible pair with F (Sykes 1988)
F	-4 to -6.5	Possible pair with E (Sykes 1988)
G	6.5 to 8	Possible pair with H (Sykes 1988).
H	-5.5 to -8.5	Possible pair with G (Sykes 1988).
J	12.5 to 15	Probable pair with K (Sykes 1988). Associated with Io family (Sykes 1989).
K	-13 to -16	Probable pair with J (Sykes 1988). Associated with Io family (Sykes 1989).
M	15 to 17.5	Probable pair with N (Sykes 1988).
N	-17 to -20	Probable pair with M (Sykes 1988).

Table II. Asteroid Family Proper and Forced Orbital Elements

Family	a	δa	e	δe	e_f	i	δi	i_f	Ω_f	$\tilde{\omega}_f$
Themis	3.137	0.025	0.153	0.009	0.038	1.420	0.223	1.22	97.8	8.7
Koronis	2.875	0.018	0.049	0.006	0.037	2.118	0.081	1.16	96.1	6.2
Nysa	2.446	0.020	0.162	0.009	0.036	3.205	0.154	0.93	86.9	351.7
Flora	2.193	0.008	0.138	0.006	0.048	5.024	0.452	0.61	43.4	338.2
Eos	3.015	0.006	0.071	0.008	0.037	10.12	0.710	1.19	97.1	7.6
Io	2.650	0.035	0.143	0.009	~ 0.06	13.36	0.240	1.06	93.9	~ 32
Maria	2.550	0.013	0.089	0.009	0.035	15.21	0.170	1.03	91.0	354.2

Table III. Asteroid Family Formation Estimates

Family	Minimum Parent Body Diameter (km)	Minimum Age (years)
Themis	300	1.5×10^9
Koronis	90	1.3×10^8
Nysa	200	2×10^9
Eos	189	5.8×10^8

Figure Captions

Figure 1. Brightness profiles for an IRAS scan on 1983 June 24 at elongation $91°.1$ (Hauser *et al.*, 1984). The ecliptic plane is crossed at longitude $1°.3$. The galactic plane is crossed near ecliptic latitude $+60°$ and galactic longitude $l = 96°.8$. All discrete features are from real sources. The prominent source near the south ecliptic pole at 60 and 100 μm is the Large Magellanic Cloud. At 12 μm and 25 μm the thermal emission is dominated by a broad zodiacal component while galactic emission dominates at the longest wavelengths. The arrows indicate bumps in the profile corresponding to the γ bands.

Figure 2. The 25μm IRAS scans have been segregated into (a) HCON 2 and (b) HCON 3, and zero-sum high-pass filtered along the in-scan direction using a filter width of $3°.5$. The data has been binned into $0°.5 \times 0°.5$ pixels and mapped in ecliptic cylindrical coordinates. Because of the separation of only ~ 10 days, HCON 1 (not shown) and HCON 2 images are nearly identical. The dust band structures are described in Table 1. $A - D$ are Type II dust trails, T2DT and EDT denote the Tempel 2 and Encke dust trails, respectively, and GC indicates galactic cirrus. The galactic plane is seen crossing the ecliptic near $90°$ and $270°$ ecliptic longitude (Sykes 1988).

Figure 3. (a) The particle number density distribution in a radial cross section of a Koronis dust band torus whose particles have orbital elements equal to the mean values of the Koronis asteroid family (with no dispersion in elements). The Sun is to the left. The jagged edges are an artifact of sampling. (b) Convolution by Gaussian dispersions in proper inclination (1σ) and semi-major axis (2σ) of the model Koronis torus increases the volume of the torus, particularly in the radial direction, while separations between peaks densities at perihelion and aphelion decrease both radially and in latitude (Sykes 1989).

Figure 4. (a) The latitudinal profile of the dust bands are shown after being convolved with a gaussian distribution of orbital inclinations with standard deviation δi. Increasing dispersion in inclination results in decreasing latitudinal separation of the dust bands and decreasing contrast between the band peaks and centers. Δ_0, Δ_+, and Δ_- indicate the shift of peak and band edge latitudes, respectively, and are defined in the text. The mean elements of the particles remain unchanged. (b) Radial profiles of the particle number density of a model torus associated with the Koronis asteroid family are shown for different dispersions in semimajor axis and (c) eccentricity. Densities are normalized to the value at $a = 2.875$ AU. The 1σ values correspond to the standard deviation of those terms over the orbits of known family members (Table II, calculated from Williams 1979). Increasing dispersion in both terms results in a decrease in the radial separation of the perihelion and aphelion bands, as well as a decrease in their contrast. The mean elements of the particles are unchanged (Sykes 1989).

Figure 5. (a) Variation of the ecliptic latitude of a dust band with ecliptic longitude, as measured in a sun-centered coordinate system. The latitudinal width of the band at all

longitudes is $2i'$, twice the proper inclination of the dust particle orbits. The amplitude of the apparent sinusoidal variation is determined by the forced inclination, i_f. (b) Variation of the forced inclination i_f and the corresponding longitude of the ascending node Ω_f with semi-major axis. The elements with subscript J are the present orbital elements of Jupiter. (c) Plane view of the distribution of elliptical particle orbits in a dust band. To order e, the figure is circularly symmetric about the point C which is displaced from the sun by an amount ae_f in a direction opposite to that of the forced pericenter, $\tilde{\omega}_f$. (d) The variation of the forced eccentricity e_f and the corresponding longitude of the forced pericenter, $\tilde{\omega}_f$, with semi-major axis (Dermott et al., 1985).

Figure 6. The total surface area of particles contained within a sphere of equivalent radius, R_e, is shown for a range of power law distribution index, q, and the lower cut-off in the particle size distribution, r_{min}. The horizontal line shows the area for the central dust band, inferred from Low et al.(1984) (Dermott and Nicholson 1989).

Figure 7 Variation of the latitude of the center (measured between the half-power points) of the central dust band as with day of the year, as seen at 25 μm in the IRAS Zodiacal History File. Data obtained when IRAS was in the leading or ascending leg of its motion around the earth are represented by squares, while the data from the trailing or descending leg are represented by triangles. The vertical lines give the forced inclination of the central band and the location of the nodes (Dermott et al.1988).

Figure 8 Geocentric ecliptic coordinates of the north and south β bands as measured from unfiltered IRAS skyflux plates (25 μm). The latitude of each band-pair component was binned and averaged every $0°.5$ in longitude (filled circles). North and South bin values were then averaged (open circles) in order to determine the geocentric ecliptic longitude of the ascending node as seen in both HCON 1 and HCON 3, roughly eight months apart. The earth's longitude, $\lambda_\oplus$, is given for the times of plane-crossing observations. HCON 1 observations plotted were made in the direction opposite to the earth's motion, while the HCON 3 observations plotted were made in the direction of earth's motion (Sykes 1989).

Figure 9 An observed dust band profile (smooth curve), after high-pass filtering, is compared with the prediction of a model based on the distribution of orbits in the Eos and Themis families (Dermott and Nicholson 1988).

Figure 10 (a) An IRAS skyflux map (Plate 95, 25μm) has been boxcar high-pass filtered, using a filter width of 1° along the scan direction, allowing the α and β bands to be distinguished. The edges of model (b) Koronis and (c) Themis dust bands are then projected onto the skyflux map for comparison with the observed bands (Sykes 1989).

Figure 11. The longitudes of the ascending nodes of an ensemble of collisional debris orbits are increasingly dispersed due to differences in semi-major axes among the debris after ejection. Nodal dispersion as a function of time is shown for different mean ejection velocities in the inner (a) and outer (b) part of the asteroid belt. When the nodes have been distributed over 360°, band formation is complete. Band formation is more rapid in the outer belt due to the closer proximity of Jupiter (Sykes and Greenberg 1986).

Figure 12. The ascending nodes of debris orbits from a single collisional event are shown as a function of time. Poynting-Robertson drag coupled with Jovian gravitational perturbations acts to decrease the rate of orbital precession by small particles relative to large particles by decreasing their semi-major axes with time. This results in band pair formation by mass fractionation of debris orbits. The distribution of ascending nodes by this mechanism (thin curves) and by the initial dispersion of semi-major axes (thick curves) are shown at different times for a single collision in the inner (a) and outer (b) part of the asteroid belt. Particle mass densities of $\rho = 3$ g/cm^3 are assumed, and a dispersion in ejection velocities of 100 m/s. For reference, the inner circle represents the orbit of earth. As in Figure 11, band pair formation in the outer belt is more rapid than the inner belt due to the closer proximity of Jupiter (Sykes and Greenberg 1986).

Figure 13(a) Debris from the catastrophic disruption of an asteroid has an initial size-frequency distribution which subsequently (b) undergoes collisional redistribution of its mass from larger to smaller particles until, eventually, particles are small enough that they are rapidly removed by radiation forces from the ensemble comprising a dust band torus. (c) The surface area of dust band tori gradually diminishes with time. The differing rates of change in surface area at different times is a consequence primarily of particle collision lifetimes which change with particle size. As time progresses, larger particles begin to be comminuted, supplying the smaller particle population at different rates (Sykes and Greenberg 1986).
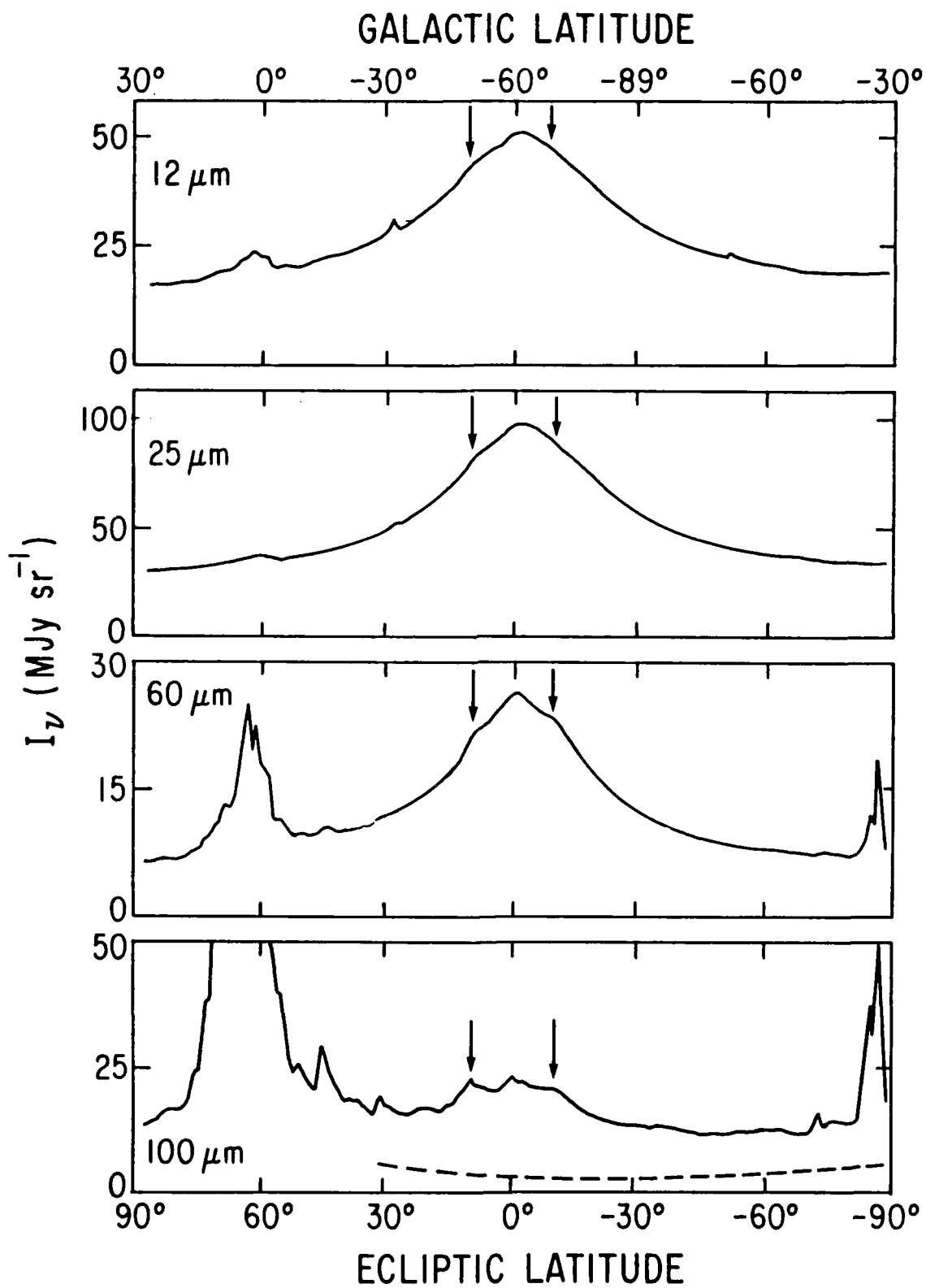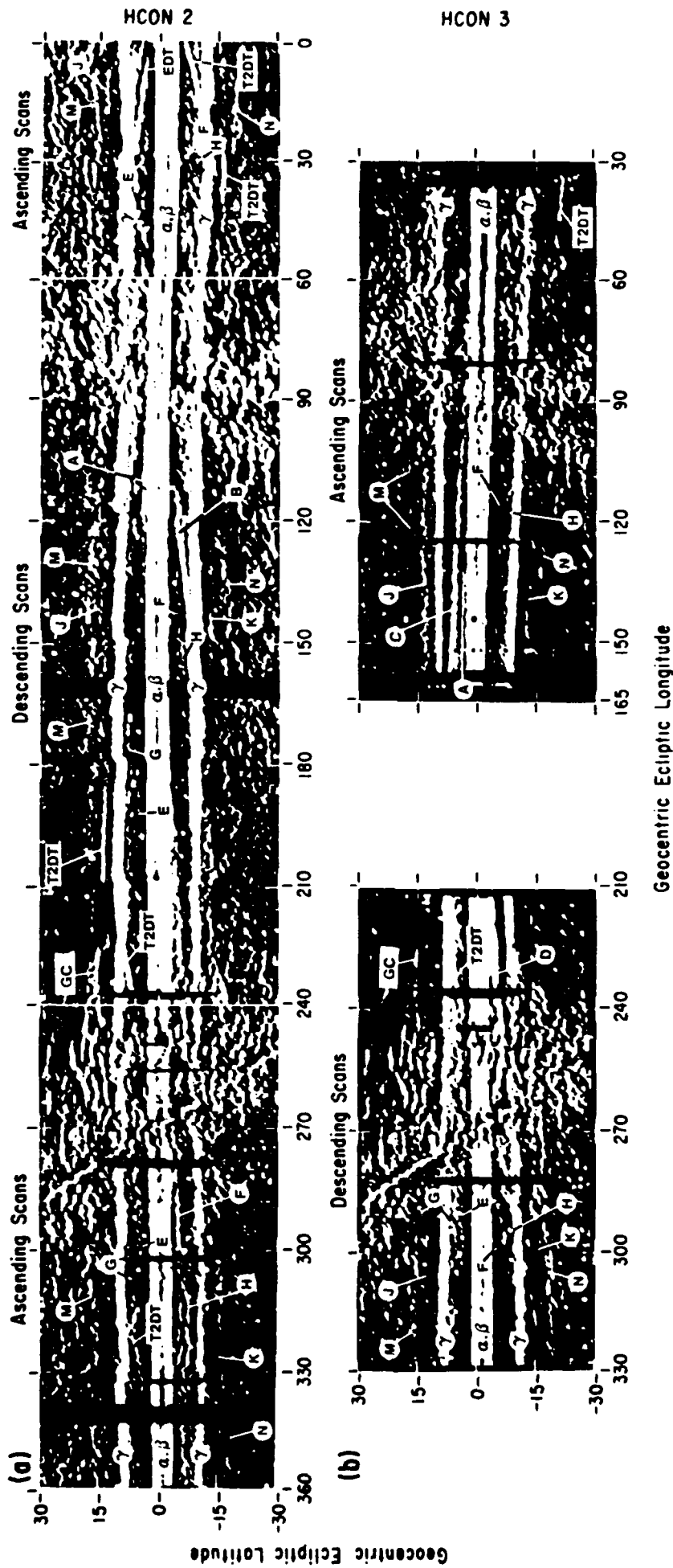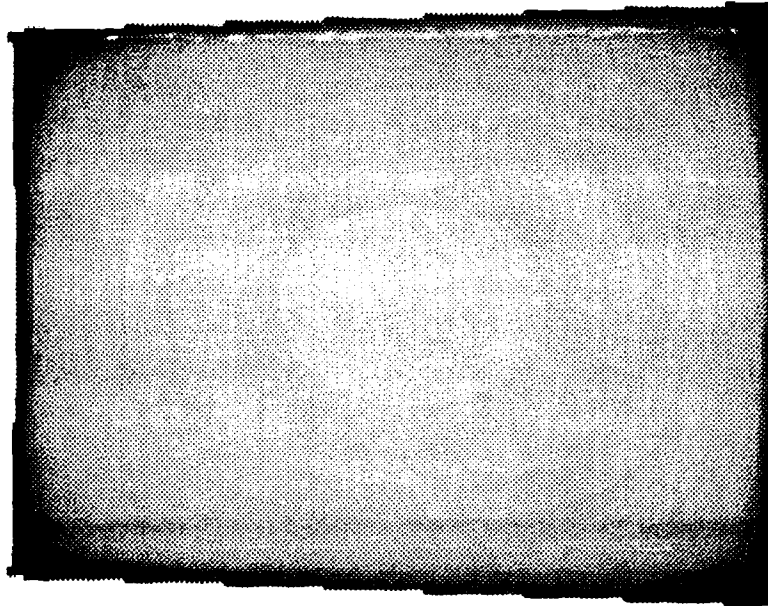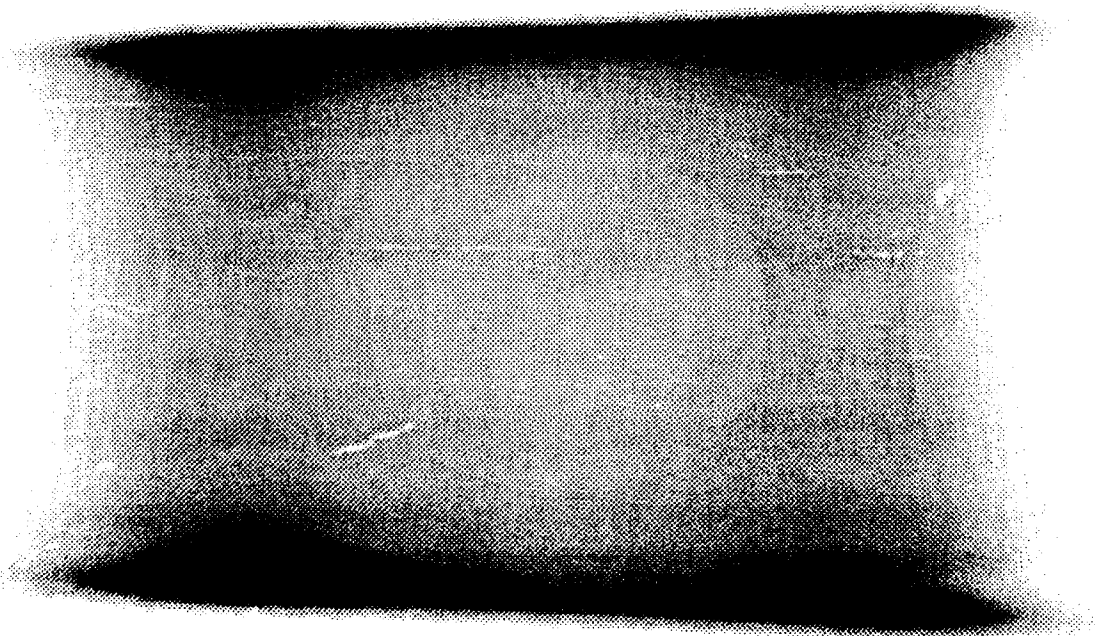
Fig. 1

GALACTIC LATITUDE

30°   0°   -30°   -60°   -89°   -60°   -30°

12 μm

25 μm

60 μm

100 μm

I_ν (MJy sr^{-1})

ECLIPTIC LATITUDE

90°   60°   30°   0°   -30°   -60°   -90°

Fig. 2

Fig. 3

(a)

(b)

Fig. 4

Fig 5

(a)

Heliocentric Ecliptic Latitude (degrees)

Heliocentric Ecliptic Longitude

0   180   360

Ω_f

I_f

$2I'$

(b)

Forced Inclination, I_f (degrees)

Ascending Node, Ω_f

Semimajor Axis (AU)

2   3   4

340   20   60   100

Ω_J

Ω_f

I_J

I_f

(c)

$\widetilde{\omega}_f$

S

C

D

$2r'$

p

(d)

Forced Eccentricity, e_f

Pericenter, $\widetilde{\omega}_f$

Semimajor Axis (AU)

2   3   4

0.08   0.06   0.04   0.02   0

340   20   60   100

e_J

$\widetilde{\omega}_J$

$\widetilde{\omega}_f$

Fig. 6

Fig 7

Fig 8

Fig.9

25μm

ℓ = 49.37
ε = 92.26

Flux Density (10⁶ Jy/sr)

Ecliptic Latitude (degrees)

Fig. 10
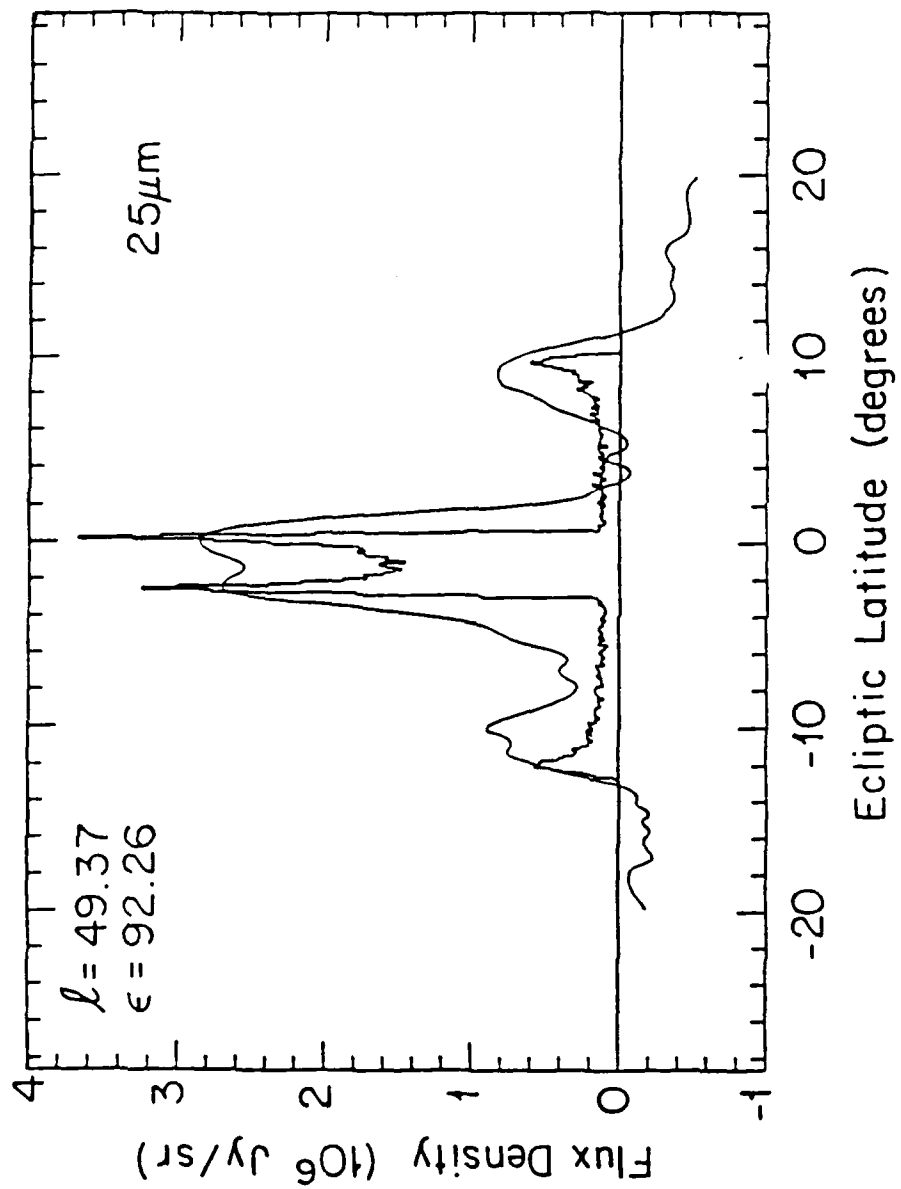
(a)
Encke dust trail
α Bands
β Bands
Tempel 2 dust trail

(b)
1°
Model Koronis Bands

(c)
Model Themis Bands

Fig. 11

Fig. 12

Fig. 13